Materials Science & Engineering A xxx (xxxx) xxx

Contents lists available at ScienceDirect

Materials Science & Engineering A

journal homepage: http://www.elsevier.com/locate/msea

Effect of hydrogen on mechanical properties and fracture of martensitic carbon steel under quenched and tempered conditions

Nirosha D. Adasooriya [a,*], Wakshum Mekonnen Tucho [a], Erlend Holm [a], Terje Årthun [a], Vidar Hansen [a], Karl Gunnar Solheim [b], Tor Hemmingsen [a]

[a] University of Stavanger, Department of Mechanical and Structural Engineering and Materials Science, Stavanger, N-4036, Norway
[b] Subsea 7, Kanalsletta 9, NO-4033 Stavanger, P.O. Box 205, NO-4065, Stavanger, Norway

ARTICLE INFO

Keywords:
Martensitic steel
Hardness
Hydrogen embrittlement
Slow-strain rate tensile test

ABSTRACT

The change in the mechanical properties of tempered high strength carbon steel (AISI 4130) due to hydrogen embrittlement (HE) has been investigated using slow strain rate tensile tests (SSRT). The heat treatment processes consisted of austenitization at 873 °C for about 45 min before quenching in salt bath and tempering at temperatures between 350 °C to 550 °C for about 1 h. The SSRT tests were performed on both hydrogen precharged and uncharged samples. Vickers hardness test was carried out to study the variation in hardness with the tempering temperature. Transmission Electron Microscopy (TEM) and Scanning Electron Microscopy (SEM) were performed for Microstructural characterizations and fracture surface analysis. The fracture surface analysis shows a transition of failure mechanism from brittle intergranular cracking at the lowest tempering temperature to ductile micro void coalescence at the highest temperature. TEM analysis reveals formation of carbide precipitates of the samples which were tempered. The AISI 4130 was subjected to HE for hydrogen charging when the tempering temperatures were 430 °C and lower, corresponding to a hardness value of 450 HV and greater.

1. Introduction

High-strength steels such as AISI 4130 have been widely used in different structures, structural components and mechanical systems within many fields, such as construction, oil and gas, aviation, agriculture and defense. To improve ductility, post heat treatments are common processes for such high strength martensitic steel. Even though much improvement has been achieved through heat treatments, many failures of high strength steel structures are still observed. The suspension cable wire fractures of Lysefjord bridge [1], Lake Maracaibo bridge and Hamburg bridge [2,3] are examples of these failures. About 40% of the failures of oil and gas pipelines are due to corrosion associated with environment-assisted cracking (EAC) [4]. Most of the research in this area focuses on EAC due to the combined effect of the inherent nature of corrosion and loading [5–7]. Corrosion is one of the principal deterioration processes that affects the integrity of steel structures. Thickness reduction, surface roughness and cyclic loading accelerate the crack initiation under different types of corrosion. There are three major types of EAC [8]: stress corrosion cracking (SCC), hydrogen embrittlement (HE) and corrosion fatigue (CF). The SCC is generally defined as failure caused by continuously applied stress in corrosive media. Fractures due to cyclic stress in corrosive media are designated as CF. The EAC is considered one of the main causes of the degradation of steel structures.

Hydrogen embrittlement (HE) in metals leads to cracking and may cause catastrophic failures. HE is often classified as (i) internal hydrogen embrittlement, which occurs due to pre-existing hydrogen in the material, or (ii) hydrogen environment embrittlement, which occurs due to hydrogen picked up from the environment under cathodic protection or presence of hydrogen gases [9]. In steel, HE may reduce ductility, toughness, strength and accelerate crack growth [9]. The HE of steel is a function of concentration of the formed hydrogen, temperature, stress state and microstructure of the material [8–10]. On the other hand, the susceptibility to HE is material dependent and there are no generalized guidelines to control the HE of high strength steels. However, HE susceptibility is decreasing with increasing tempering temperature for martensitic steel (i.e. a decrease in hardness) [8].

In some structural materials manufactured as-quenched or under tempered conditions, precipitated carbides may reduce the hydrogen diffusivity in the materials and cause intergranular fracture [11]. The formation of carbide precipitates is dependent on factors such as carbon content, cooling rate, quenching media and tempering temperature

* Corresponding author.
E-mail address: mudiyan.n.adasooriya@uis.no (N.D. Adasooriya).

https://doi.org/10.1016/j.msea.2020.140495
Received 19 December 2019; Received in revised form 3 November 2020; Accepted 4 November 2020
Available online 9 November 2020

Abbreviations

CF	Corrosion fatigue
CNC	Computer numerical control
EAC	Environment-assisted cracking
HD	Hydrogen damage
HE	Hydrogen embrittlement
HV	Vickers hardness value
I_{HE}	Relative HE susceptibility index
SEM	Scanning Electron Microscopy
TEM	Transmission Electron Microscopy
SCC	Stress corrosion cracking
SSC	Sulfide stress cracking
SSRT	Slow strain rate tensile tests

[11–14].

The effects of internal HE on steel have been studied in terms of loss of ductility with intergranular cracking and work hardening [8,9,15,16]. These processes depend on the strain rate, the method of hydrogen charging and the microstructure of the material [8,17–21]. The two most used experimental hydrogen charging methods are electrochemical (i.e. cathodic protection) and exposure to hydrogen gas [8]. Slow strain rate tensile tests (SSRT) are often used for HE susceptibility investigations of steel [22]. In order to avoid HE, the NORSOK standard recommends the use of a material with a hardness of 350 HV or lower or use of a steel with low carbon content for structural/mechanical parts/components that are cathodically protected [23]. Even though, standards have their merit in an industrial context, several different microstructures can make-up for the same hardness yet cause a different behaviour with respect to the interaction with hydrogen. The HE susceptibility depends on the material, environment and application. Therefore, case specific investigations are required in order to determine HE susceptibility limits.

AISI 4130 steel with 620 MPa yield strength is considered as one of the suitable materials for use in a hydrogen sulfide environment [24]. The effects of anisotropy on the hydrogen diffusivity and stepwise cracking of AISI 4130 steel with a banded ferrite/pearlite structure have been studied by Gao et al. and Lee et al. [25,26]. They found similar hydrogen diffusivity levels in longitudinal and in transverse directions in the materials. On the other hand, the effect of hydrogen on the fatigue strength of quenched and tempered AISI 4130 steel showed a variation in crack propagation, and toughness values were deeply influenced by the presence of hydrogen [27,28]. The effect of HE during fracture toughness test of quenched and tempered AISI 4130 steel has been simulated by a three-step procedure using the simulation software by Gobbi and Vergani [29]. From their study, Gobbi and Vergani [29] proposed a cohesive model that simulate the effects of HE on fracture toughness. The reliability of the simulation was proved by a sensitivity analysis. The electro metallization of an aluminum coating was proposed to ensure the reliable operation of oil and gas equipment made by AISI 4130 hull steel [30]. Even though several studies have been carried out on AISI 4130, there is still a lack of investigations concerning the relationship between the HE susceptibility and hardness and also tempering temperature for cathodically protected AISI 4130 steel. In addition, the limiting/conservative values for tensile strength and fracture strain (i.e. ultimate fracture strain) are not available for cathodically protected tempered AISI 4130 steel.

The objective of this study is therefore to investigate the HE susceptibility of tempered high strength carbon steel, AISI 4130 by SSRT of hydrogen pre-charged samples under hydrogen charging while straining. The samples were first austenitized and quenched to martensitic structure, then tempered to improve the ductility and reduce the hardness. Before performing SSRT at strain rate of $1x10^{-6}s^{-1}$ under hydrogen charging, the specimens from the different tempering state were pre-charged with hydrogen. The microstructure and fracture surfaces of the tested specimens are studied. The relationship between the HE susceptibility and hardness are also analyzed and presented.

2. Materials and experimental procedure

2.1. Materials

The chemical composition of the high strength carbon AISI 4130 steel used for this work is given in Table 1. For tensile testing, 24 samples were prepared according to ASTM E8 standard [31]. The geometry of the samples is shown in Fig. 1. The samples were austenitized at 873 °C for 40–50 min and rapidly transferred into a salt bath maintained at 180 °C for quenching. An agitator in the salt bath provides an extra cooling effect by circulating the salt. To minimize the risk of bending during quenching, the samples were submerged in a vertical position.

The samples were divided into three groups, each consisting of 8 samples, as shown in Table 2. The samples from one of the three groups were tested only in air. The as-quenched sample of this group is labelled as AQ, whereas A-xx (i.e. xx represents tempering temperature) represent the tempered samples. The other two groups were subjected to hydrogen charging and the samples are suffixed as H1and H2, respectively. H1Q and H2Q stand for as-quenched hydrogen charged samples of the two groups. H1-xx and H2-xx represent tempered samples of the hydrogen charged of the two groups and xx represents tempering temperature. The description of the samples together with some of the measured data are shown in Table 2.

2.2. Electrochemical hydrogen charging

Samples in H1 and H2 groups were charged with hydrogen for approximately two weeks' duration under similar conditions as shown in Table 2, prior to SSRT. The hydrogen charging was not started at the same time for all samples to maintain consistency of charging time between samples after taking the SSRT test time into account. The charging times were started during three consecutive days for each group of samples. The fully saturation of hydrogen can be achieved for all the AISI 4130 steel samples during approximately two weeks of charging period [26,29,33]. Though fully saturation of hydrogen charging has been reported for AISI 4130 steel in shorter time [26], authors decided to consider approximately two weeks duration to get the effect/damage due to longer charging time, which is the common situation for CP of offshore structures/pipelines. The test samples would be saturated with hydrogen during this incubation period. A 20L square plastic container with the capacity of holding 16 samples was filled with 3.5 wt% NaCl in distilled water as electrolyte. The NaCl electrolyte was particularly chosen to simulate the marine environment. The set up for pre-charging included an AISI 4130 sample as working electrode (tensile samples), an Inconel 625 steel (58 wt% nickel) bar with approximately same surface area as the samples as a counter electrode, and a saturated calomel electrode (SCE) (radiometer analytical probes, REF201) as a reference electrode. A Labor-Netzgerat EA-3021S was used as a power supply and a Hioki 3803 digital multimeter was used for controlling the voltage with reference to the SCE. The voltage was set at −1050mV (±50 mV) SCE for the entire hydrogen charging period of the samples. There was no interference between the samples that are charged in the same container in terms of applied potential. The electrolyte was changed four times during the incubation period in order to maintain the composition of the electrolyte.

2.3. Slow strain rate tensile test

In order to determine the effect of hydrogen charging on mechanical and fracturing properties, an experimental set up shown in Fig. 2 (a) was used for the SSRT tests. The setup consisted of electrochemical cell,

Table 1
The chemical compositions of AISI 4130 (in wt%).

C	Si	Mn	P	S	Cu	Cr	Ni	Mo	V	N	Al	Nb	As	Sn	Ti	Co	Ca	Fe
0.31	0	0.5	0.01	0	0.2	1.1	0.1	0.2	0.004	0.006	0.023	0	0.01	0.01	0.003	0.01	1	Bal.

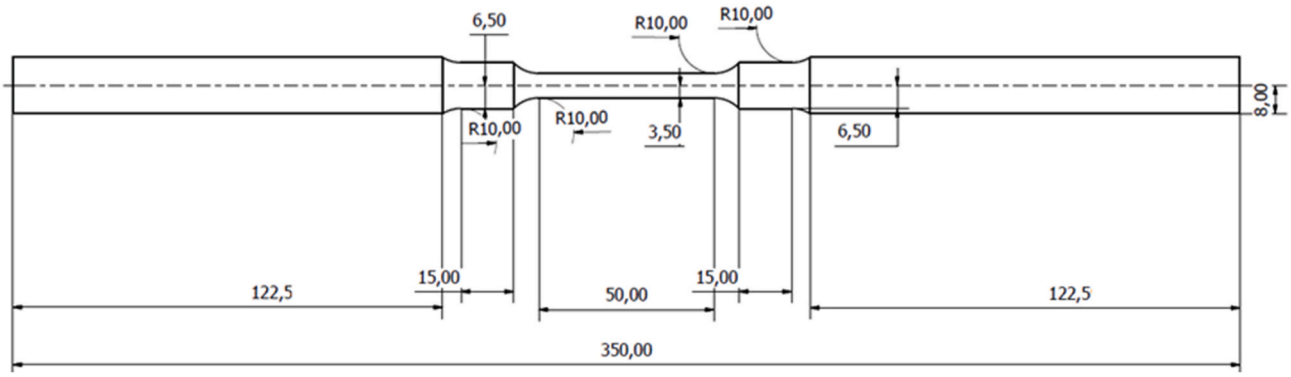

Fig. 1. Dimensions of the tensile test sample in mm.

Table 2
The samples studied, average hardness and SSRT test results.

Sample Designation	Tempering temperature (°C)	Hydrogen charging duration (hrs)	Hardness (HV)	Tensile strength (MPa)	Fracture strain/Strain to failure	Reduction of area (%)
AQ	quenched	0	557 ± 9	2049	0.0943	39
A-350	350	0	490 ± 5	1705	0.0631	–
A-400	400	0	461 ± 5	1562	0.0795	56
A-430	430	0	447 ± 4	1282	0.0817	63
A-460	460	0	425 ± 3	1308	0.0964	66
A-490	490	0	402 ± 3	1125	0.0946	64
A-520	520	0	378 ± 4	1119	0.0947	64
A-550	550	0	360 ± 4	1100	0.1144	67
H1Q	quenched	356.5	541 ± 12	1269	0.0198	3
H1-350	350	337.8	493 ± 4	1057	0.0137	2
H1-400	400	340.6	472 ± 3	1242	0.0165	3
H1-430	430	358.3	445 ± 2	1240	0.0262	4
H1-460	460	343.9	421 ± 3	1150	0.0194	3
H1-490	490	341.8	400 ± 3	1227	0.039	8
H1-520	520	344.0	381 ± 4	1207	0.0468	11
H1-550	550	340.2	352 ± 4	980	0.0439	18
H2Q	quenched	309.7	545 ± 13	1249	0.0208	0
H2-350	350	292.6	489 ± 4	1157	0.0166	2
H2-400	400	316.6	465 ± 3	1182	0.0161	1
H2-430	430	292.5	445 ± 3	1192	0.0175	4
H2-460	460	295.0	422 ± 4	1259	0.0254	5
H2-490	490	295.9	401 ± 3	1225	0.0285	9
H2-520	520	316.6	380 ± 5	1152	0.0454	12
H2-550	550	341.4	353 ± 3	1068	0.0447	17

tensile testing machine and data acquisition system. A three-electrode cell was used in the tests as shown in Fig. 2 (b) for in-situ hydrogen charging. In a cylindrically polycarbonate plastic container filled with a 0.5 M NaCl electrolyte, each sample was potentiostatically charged under dynamic tensile load. The three-electrode cell included a tensile test sample as working electrode, an equal sized Inconel 625 bar as a counter electrode, and a saturated calomel electrode as a reference electrode. The potential was set at −1050 mV SCE by use of a Gamry interface 1010E potentiostate. The samples were mounted to an INSTRON 5985 dual column floor frames testing machine and tested at various strain rates.

For the SSRT tests, the hydrogen charged samples (−1050 mV SCE) were transferred from the incubation container to the tensile test cell within 2–3 min, in order to minimize hydrogen loss from the surface of the samples. Slow strain rate of 10^{-6} s^{-1} was applied for allowing hydrogen to migrate to crack tips during propagation [31]. The strain rate has a significant effect on the percentage reduction in area during HE [32]. Therefore, all the 16 samples in H1 and H2 groups have maintained consistency in strain rate. It is thus necessary to test all the hydrogen charged samples at unique strain rate. The tensile test for the uncharged samples were done in air (Table 2). The first two samples (i.e. AQ and A-350) were tested at the same strain rate as that of the hydrogen charged samples. The standard has not specified a strain rate for unchanged samples tested in air as there is no significant effect on uniaxial stress-strain curve. Therefore, the rest of the uncharged samples were tested in air at the strain rate of $0.0025s^{-1}$ which is within the recommended range for HE [31–33] to minimize the duration of testing time. The load versus displacement data were recorded during the test. Tensile strength reduced cross-sectional area and total elongated length were measured after the samples were fractured. The relative HE susceptibility index (I_{HE}) was calculated for the hydrogen charged samples. The I_{HE} is defined by the ratios of stress-strain curve characteristic

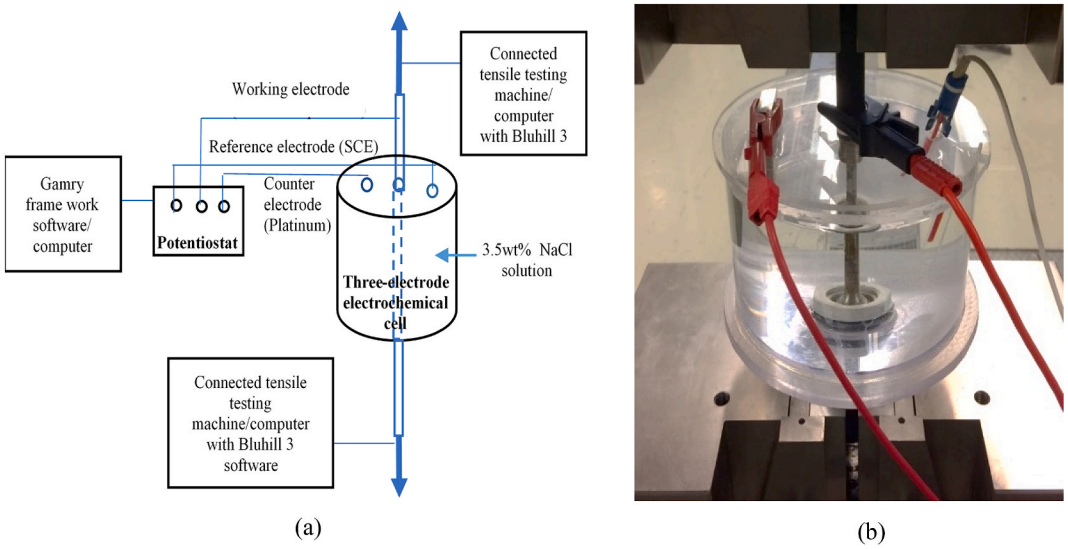

Fig. 2. (a) Schematic diagram of SSRT experimental set-up; (b) Combined electrochemical/strain cell with a three-electrode set up.

parameters of samples tested after hydrogen charging using the characteristic parameters of the samples tested in air as shown below [4,11,34,35].

$$I_{HE}\% = \left(\frac{\text{hydrogen uncharged mechanical property} - \text{hydrogen charged mechanical property}}{\text{hydrogen uncharged mechanical property}}\right) \times 100\% \quad (1)$$

$$I_{HE}\% = (1-\alpha) \times 100\% \quad \text{where } \alpha = \begin{cases} \dfrac{\varepsilon_{u,\,ch}}{\varepsilon_{u,\,uc}} \\ \dfrac{A_{ch}}{A_{uc}} \end{cases} \quad (2)$$

$\varepsilon_{u,uc}$ and A_{uc} are fracture strain and percentage reduction of cross-sectional area, respectively of the uncharged samples tested in the air. $\varepsilon_{u,ch}$ and A_{ch} are stress-strain curve characteristic parameters of the hydrogen charged samples. The $\varepsilon_{u,uc}$, A_{uc},$\varepsilon_{u,ch}$ and A_{ch} are the measured mechanical properties for I_{HE}.

Generally, the behaviours of test specimens were subjected to variations including the material microstructure. This can be captured by testing many samples under the same conditions and plotting the probabilistic distribution functions. Hence one can determine the characteristic conservative values for the parameters by considering mean minus certain amount of standard deviations. This is quite impossible as eight different tempering temperatures (i.e. eight different microstructural conditions) have been considered. Therefore, conservative limiting values are predicted in the latter part of this paper based on the plots with best fit curves to overcome the mentioned uncertainties of the calculated HE susceptibility indices. It is also well known that partial safety factors are generally used to take into further account these material uncertainties in almost all the safe design practices.

2.4. Hardness test

Hardness is one of the material properties that could give an indication of how susceptible a material is to hydrogen embrittlement. The measurement with Vickers hardness was done on samples extracted from each of the quenched and tempered samples. The samples for the test were prepared by grounding and polishing with up to 2000 grit emery paper. The hardness was calculated from 24 indentations for each sample according to NS-EN ISO 6507 [36].

2.5. Microscopy

The microstructures of the samples and fracture surfaces were studied using Scanning Electron Microscopy (SEM), Gemini SUPRA 35VP (ZEISS). The sample extracted from fracture surfaces of tested samples were cleaned with acetone and their fracture morphologies were observed by SEM. For microstructure studies, selected samples were prepared from both charged and uncharged groups (Table 2). Sample preparation for the microstructure investigations with SEM consisted of mechanical grinding, fine polishing and etching based on Struers application notes [37]. The etching was performed with LectroPol-5 electro-polishing system using A2 electrolyte at 40 kV, for a duration of about 12 s.

Finer details of the microstructure, including phases and defects, were further investigated with Transmission Electron Microscopy (TEM), JEOL-2100 (LaB_6 filament), operating at 200 kV. The investigations with TEM were performed on selected samples: HQ1, H2-400, H1-490, H1-550, AQ and A-490 (Table 2). For the TEM analysis, thin foils were prepared, first by thinning down mechanically to a

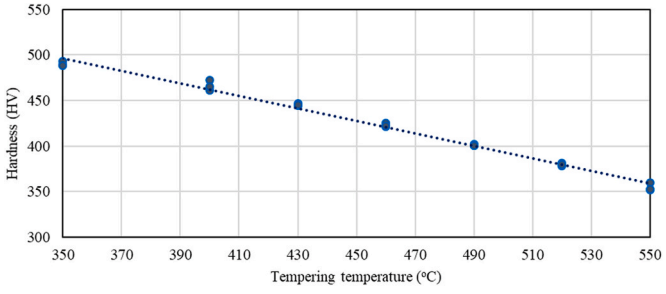

Fig. 3. Hardness as a function of tempering temperature of the AISI 4130 steel.

thickness of about 100 μm, and then punched 3 mm disks from the foils. These disks were then electro-polished using a dual jet polishing system, Struers TENUPOL-5 operated at 13 V and at −30 °C in an electrolyte solution of 95% methanol and 5% perchloric acid.

3. Results

3.1. Hardness

The average hardness measured is tabulated in Table 2. In addition, the plot of hardness as a function of tempering temperature is given in Fig. 3. The plot indicates a linear dependency of hardness in the temperature range between 350 °C and 550 °C, corresponding to hardness between 557 HV and 353 HV respectively.

3.2. Stress-strain behaviour and mechanical properties

Numerical values of tensile strength, fracture strain, percentage reduction of cross-sectional area, average hardness and hydrogen charging durations are listed in Table 2. For studying the tensile properties, the nominal stress-strain behaviour of hydrogen pre-charged and uncharged samples is given as a function of tempering temperature in Fig. 4 (a) to 4(h). The loss of ductility after hydrogen charging is clearly demonstrated in these results. The austenization heat treatment followed by quenching forms pure martensitic steel that increases the hardness and tensile strength of the material. For tempering temperatures of 490 °C and lower, the tensile strengths of the charged specimens are almost the same, i.e. about 1200 MPa. After tempering and hydrogen charging, the samples exhibited reduction in ductility and tensile strength. Ductility is however increasing with tempering temperature as shown in Fig. 4. A similar trend is also observed for the tempered specimens with maximum ductility corresponding to the highest tempering temperature.

The reduction of the cross-sectional area (*A*%) of the tensile tested samples was decreasing with decreasing tempering temperature as shown in Fig. 5(b). The hydrogen charged samples were subjected to

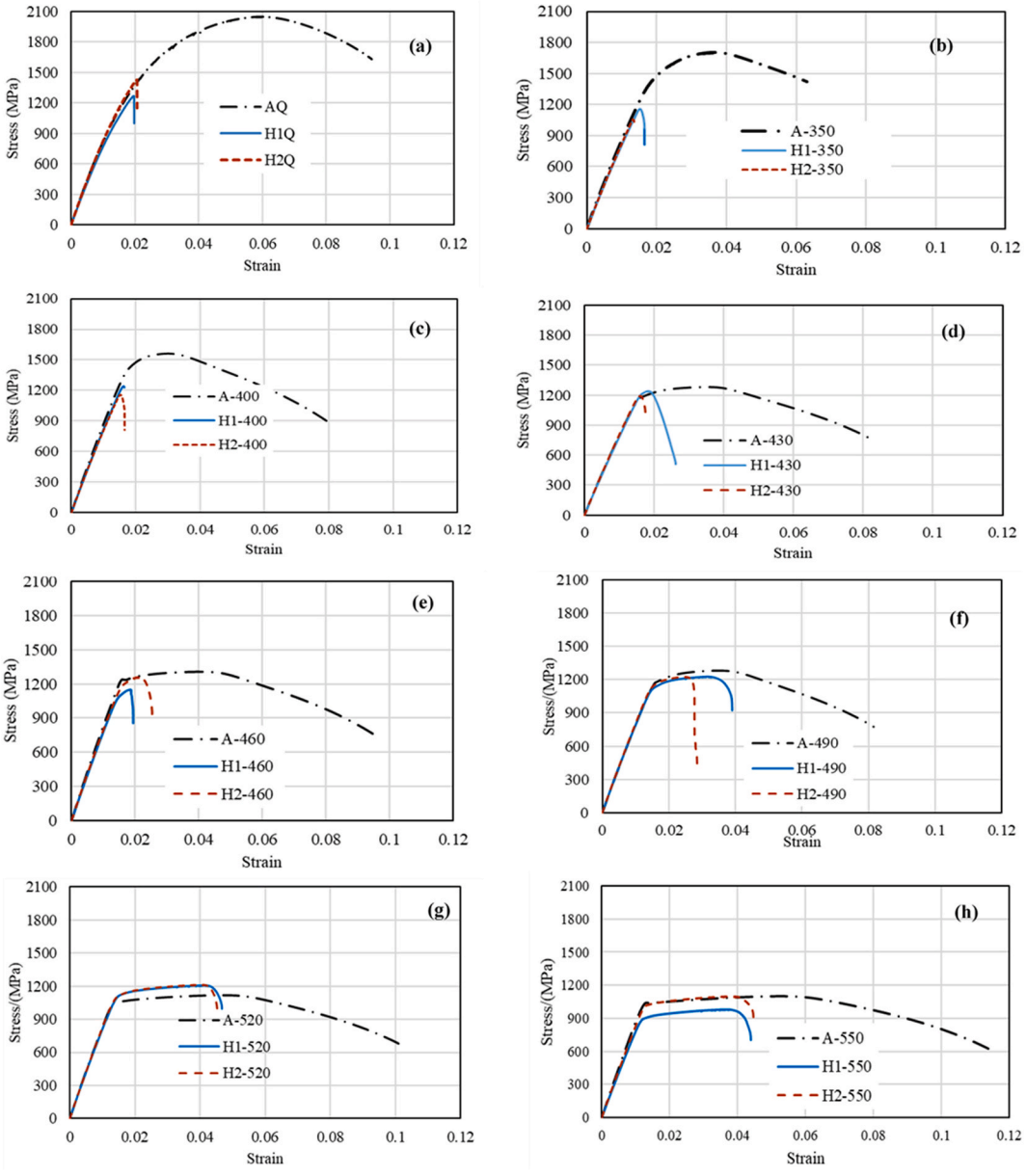

Fig. 4. Comparison of stress-strain curves of uncharged and hydrogen pre-charged samples: (a) as quenched sample, (b) using tempering temperature (TT) 350 °C, (c) TT 400 °C, (d) TT 430 °C, (e) TT 460 °C, (f) TT 490 °C, (g) TT 520 °C and (h) TT 550 °C.

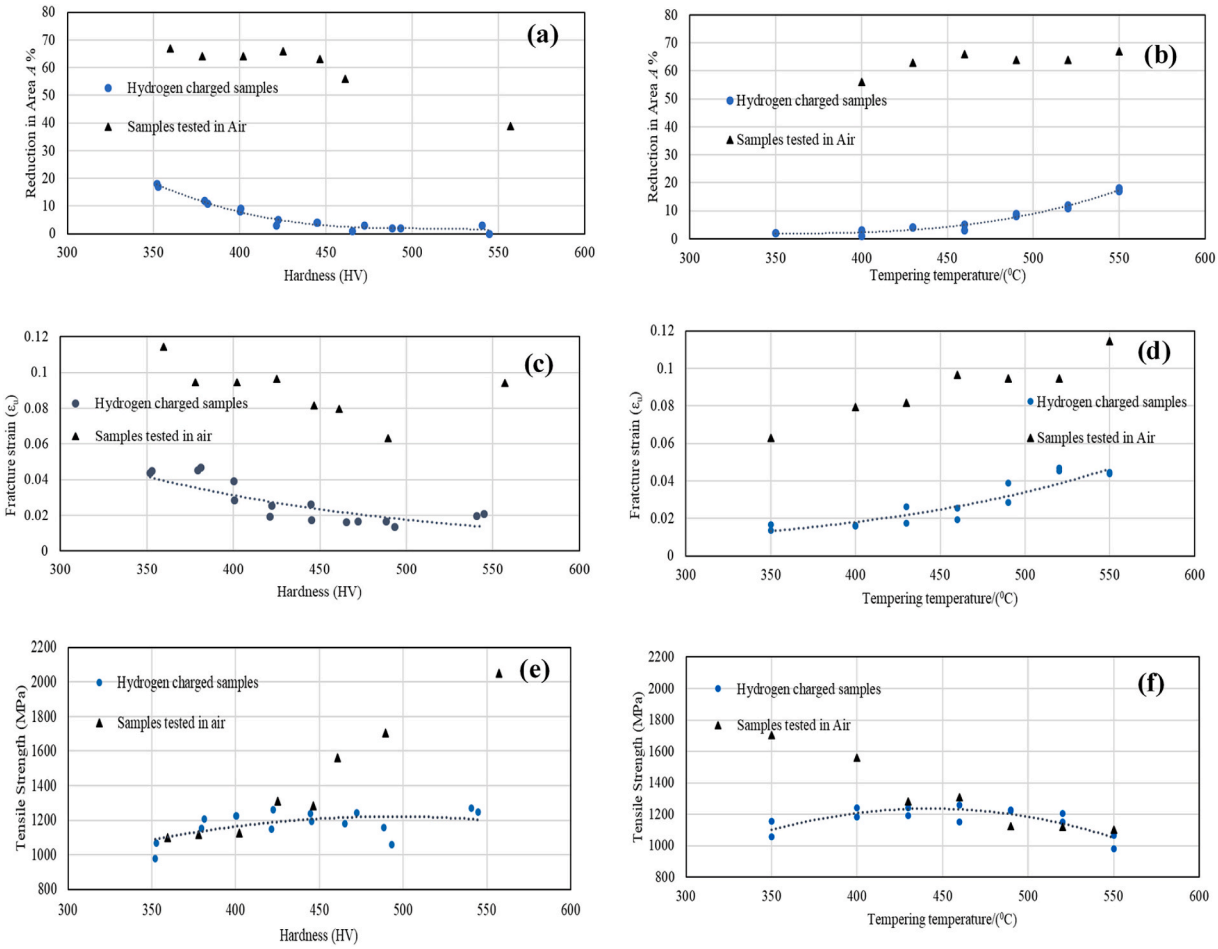

Fig. 5. (a) Reduction of cross-sectional area versus hardness, (b). Reduction of cross-sectional area versus tempering temperature, (c) Fracture strain versus hardness, (d) Fracture strain versus tempering temperature, (e) Tensile strength versus hardness, (f) Tensile strength versus tempering temperature (1 h).

significant decrement of *A*%. Negligible *A*% reduction is observed for the material tempered below 430 °C. Fig. 5(c) shows the decrement of ductility (fracture strain) with increased hardness for the samples tested in air. The fracture strain reaches a constant value when hardness is larger than 465 HV (<460 °C) for charged samples. There is a clear trend between tensile strength and tempering temperature for the samples tested in air as shown Fig. 5(f). In contrast, the tensile strength attains a constant value for the charged samples tempered below 460 °C (hardness > 450 HV). An increased tempering temperature successively reduces the tensile strength and increases the ductility, both for charged and for uncharged samples. The area reduction is significantly reduced with hydrogen pre-charging. The ductility of uncharged samples decreased for the two lowest temperatures (350 and 400 °C), and slightly increased at higher temperatures. For charged samples, the trend is opposite, almost no changes at the lowest temperatures, and a small increase for the highest.

3.3. Susceptibility of hydrogen embrittlement

The relative HE susceptibility indices (I_{HE}) are calculated for each stress-strain curve of tempered states, with respect to the characteristic parameters of the tested samples as explained in Section 2.3. The percentage reduction of cross-sectional area, tensile strength and fracture strain versus the mean HV hardness values of the samples are plotted and shown in Fig. 5(a)–5(c). I_{HE} of the fracture strain and percentage reduction of cross-sectional area (*A*%) are plotted as a function of hardness in Figs. 6 and 7, respectively.

Fig. 6 (a) shows a significant increment of HE susceptibility index of

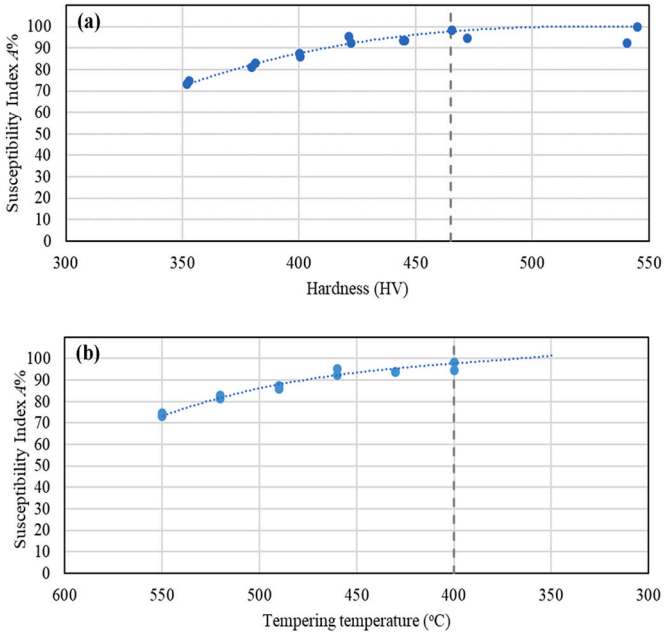

Fig. 6. HE susceptibility index of reduction of cross-sectional area of the AISI 4130 samples versus, (a) Hardness, (b) Tempering temperature.

A% with the hardness. More than 70% of HE susceptibility is observed

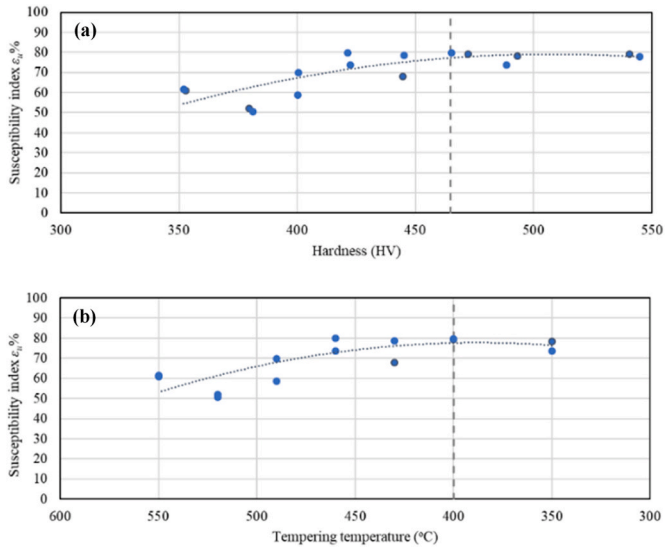

Fig. 7. HE susceptibility index of fracture strain of the AISI 4130 samples versus, (a) Hardness, (b) Tempering temperature.

for all the samples. 100% HE susceptibility is obtained for samples with hardness of 465 HV and larger. Similarly, a 100% HE susceptibility can be seen for the samples heat-treated below 400 °C tempering temperature as shown in Fig. 6(b). Fig. 7(a) shows the increment of HE susceptibility index of fracture strain with the hardness. HE susceptibility is larger than 50% for all the tested samples. About 80% of HE susceptibility is observed for material with hardness larger than 465 HV. This suggests that the AISI 4130 material is most likely subjected to HE due to hydrogen charging when the hardness is larger than 465 HV. It is also accompanied with loss of ductility. Similarly, Fig. 7(b) shows around 80% of HE susceptibility for the samples which were tempered at temperatures lower than 400 °C. Both Figs. 6 and 7 conclude that AISI 4130 is more than 80% susceptible to HE due to the hydrogen charging when the tempering temperature is below 400 °C. In general, the HE susceptibility are decreasing with increasing tempering temperature.

3.4. Fractrography

The fracture surfaces of the tempered and hydrogen charged samples in group 2 were examined by SEM. Morphology of the fracture surfaces for three of the samples are shown in Fig. 8. These samples were tempered at 350 °C (Fig. 8(a) and (b)), 430 °C (Fig. 8(c) and (d)) and 490 °C (Fig. 8(e) and (f)). At lower tempering temperatures (Fig. 8(a)–(b)), "intergranular" surfaces with numerous secondary cracks perpendicular to the surface, following prior austenitic grain boundaries were observed as expected for brittle materials. Fig. 8(b) shows (H-350) typical intergranular type fractures that clearly follow the prior austenite grain boundaries as compared to the fractures for the H2-430 (Fig. 8(c) and (d)). The latter exhibits mainly non-intergranular type fractures. Close inspection of the images reveals that the material became less brittle with increasing tempering temperature. Fig. 8(e) and 8(f) show fracture images for the samples tempered at 490 °C (H2-430), showing mainly microcracks, with a more ductile nature. The samples tempered at 550 °C exhibit distinct dimples, which is a characteristic of plastic deformation before fracture as is seen in Fig. 8(f).

3.5. Microstructure

SEM images shown in Fig. 9 represent the air-as quenched and H1-550 in (a) and in (b), respectively. The microstructures of both images are identified as martensitic laths with packets morphology revealing the prior austenitic grains. The analysis of Electron Back Scatter Diffraction (EBSD) patterns recorded from as quenched and tempered (550 °C) samples did not give indication of the presence of retained austenite. Examples of approximate prior austenite grain boundaries are marked in the images. These grains are about 6–8 μm in size whereas the average thickness of the martensitic laths of the air-as quenched lies in the range between a few tens of nanometers to hundreds of nm.

The microstructures of the four selected states, i.e. the as quenched, and after subsequent tempering at 400 °C, 490 °C and 550 °C have been also studied with transmission electron microscopy. The TEM bright field (BF) image of the as quenched state (Fig. 10(a)) shows martensitic laths with a width ranging between 50 and 400 nm. Similar martensitic laths are also seen in the sample tempered at 400 °C as shown in Fig. 10 (b). There are some variations in contrast in the laths due to differences in orientation based on residual stress, that may largely depend on the tempering temperature. After tempering, carbide precipitates were observed along the lath boundaries (Fig. 11(a), (c) & (d)) and within the laths (Fig. 11 (b)). Tempering results in relieving of stress and formation of carbides on the precursor lath boundaries and inside the laths, named as intralath and interlath, respectively [38]. The formation of carbides reduces carbon content in the solid solution of the matrix and may lead to transformation to ferrite phase. The interlath precipitates, ~10 nm in thickness cover a considerable part of the lath boundaries. As shown in the images of Fig. 11, different types of carbides are formed. Tempering at the highest temperature, 550 °C, formed both intralath and interlath carbides. The intralath carbide precipitates at 550 °C have the same morphology as that of the 490 °C, but the interlath precipitates are rod-like (Fig. 11(b)) and irregular (Fig. 11(d)) in their shapes.

4. Discussions

4.1. Effect of tempering temperature on the mechanical properties

The results indicate that the hardness and tensile strength of the uncharged samples decrease with increased tempering temperatures, whereas ductility generally increases as expected. The highest hardness and tensile strengths are observed when the material is under as quenched condition. Quenching results in a high density of dislocation that accumulates large amounts of stresses. Stresses are relieved by annihilation of dislocations and other lattice defects depending on tempering temperature. Under the solid solution condition, carbon was homogeneously distributed in the matrix. During tempering however, carbon was decomposed to form carbide precipitates. TEM images of the samples tempered at 400 °C, 490 °C and 550 °C (Fig. 11) reveal a high density of metal carbides, confirming segregation of substantial amounts of the alloy elements during precipitation. Carbide can be precipitated at the lowest temperature, 350 °C too. Similar phenomena have been reported previously [13,39–42]. The structures of these precipitates have shown different morphologies. At 490 °C, the carbide precipitates are mixed type-interlaths as well as intralaths. The highest temperature however results in more precipitates along the boundaries of the laths (interlaths), which are considered to be less efficient in preventing dislocation movements. In addition, the interlath precipitates has spherodized, which also reduce the pin up effect by the dislocations. As for martensitic tempered steels, decreasing strength means increasing ductility.

The influence of hydrogen charging on mechanical properties can be revisited from the stress-strain curves shown in Fig. 4. Generally, the ductility of martensitic steel is increasing while hardness is decreasing as reported by many scholars too [4,39,40]. There are considerable differences in ductility between hydrogen-charged samples and uncharged samples (see for example Fig. 4(a)). The ductility of the charged sample was increased with tempering temperatures. Lattice defects, such as dislocations, are considered as the main trapping sites of hydrogen. As it is already discussed, the amount of dislocation density is decreasing with increasing tempering temperature and thus less trapped hydrogen. Therefore, low ductility corresponds with higher density of lattice

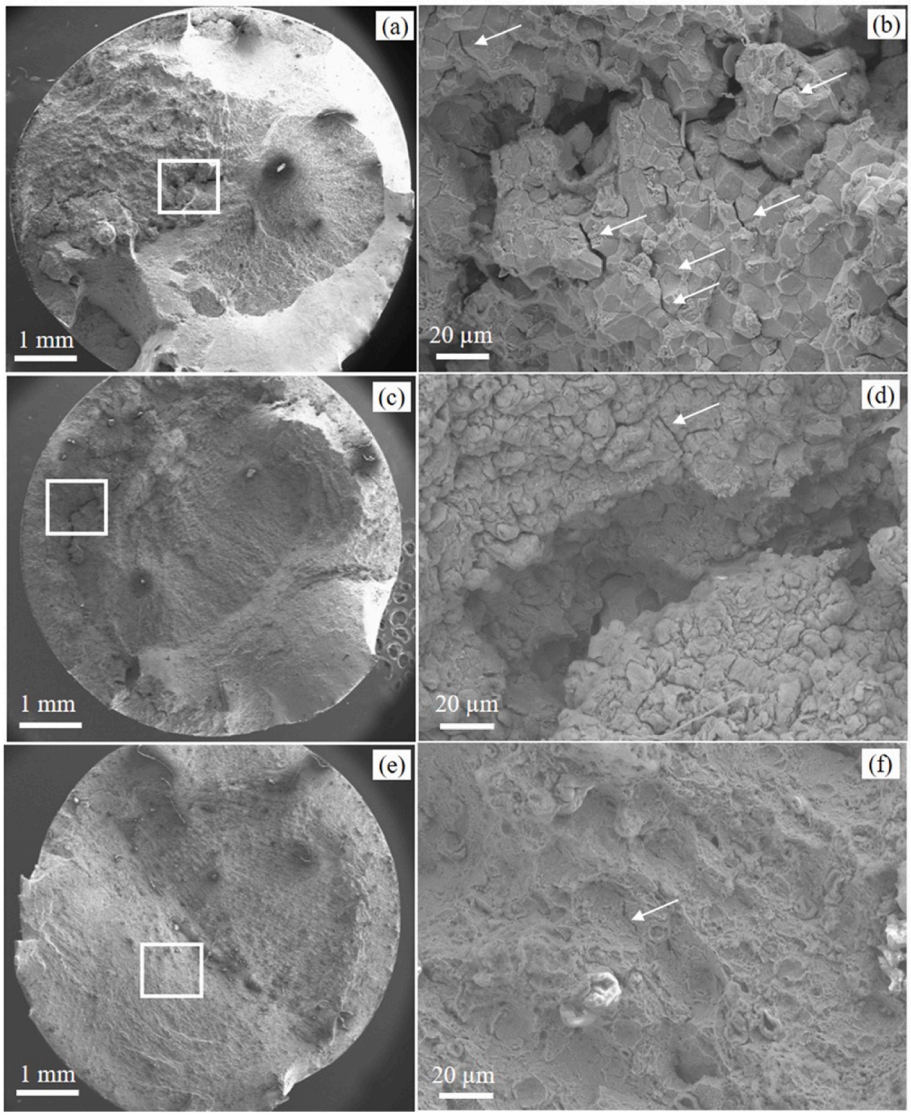

Fig. 8. Fracture surfaces of AISI 4130 in full and magnified view of (a,b) H2-350, (c,d) H2-430 and (e,f) H2-490. The magnified images are from the marked square regions of the images in full views (some of the microcracks are shown by arrows).

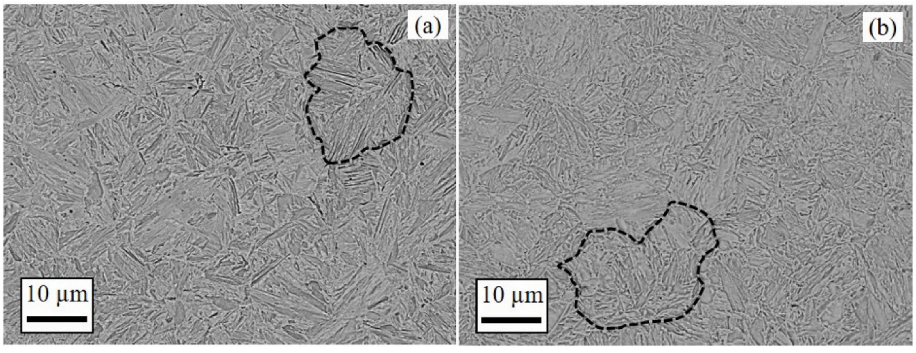

Fig. 9. SEM image of (a) air-as quenched and (b) H2-550.

defects (dislocation) that could trap large amounts of hydrogen. This may be why the material is 100% susceptible to HE when the tempering temperature is below 400 °C.

The morphology of the fracture surface can also be explained in terms of the concentration of hydrogen absorbed in the sample. As shown in Fig. 8 (section 3.4), the tendency of crack formation is higher with samples that trapped larger amounts of hydrogen, e.g. at lower tempering temperature. The microstructure of the samples tempered at lower temperature contains a high concentration of stress that can trap hydrogen to a high extent. This leads to decreasing of cohesive strength and high concentration of hydrogen in the prior austenitic grain boundaries. The grain boundaries then act as crack initiation sites that

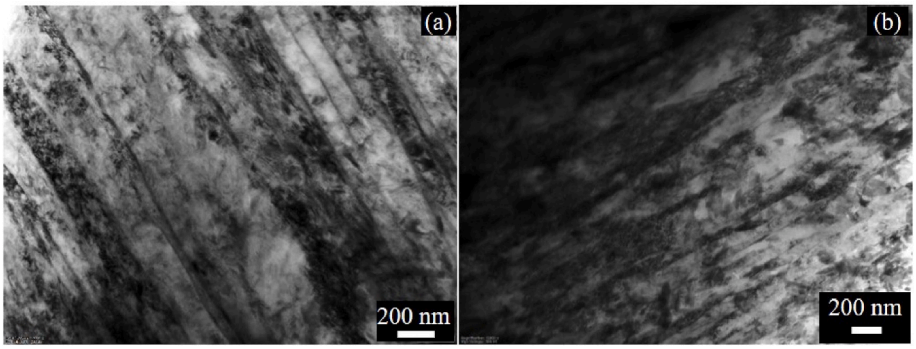

Fig. 10. TEM bright field images showing laths of martensitic structure (a) air-as quenched (b) H2-400.

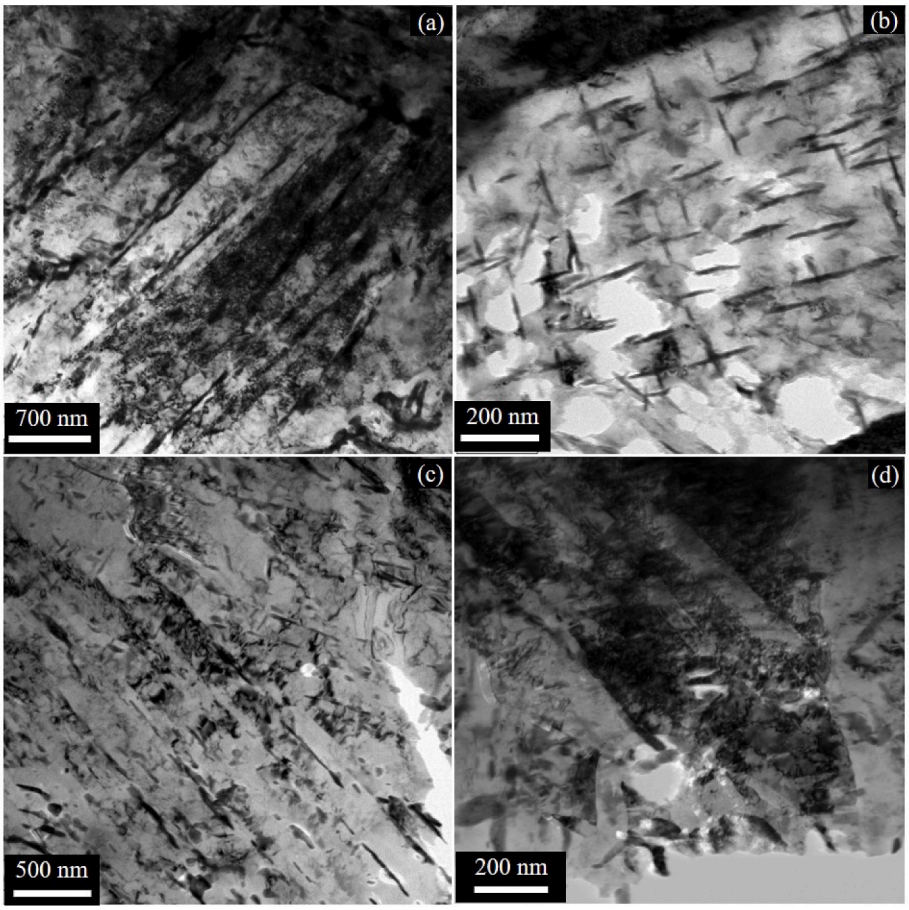

Fig. 11. Bright field TEM images of H2-490 (a, b), (c) H2-550 and (d) H2-400 showing dislocation. The carbides seen in (a) and (d) are precipitated along the lath boundaries (interlaths) whereas the carbides in (b) are precipitated within the laths (intralaths).

tend to propagate at the lowest applied stress to fracture with intergranular character. This mechanism is generally referred as hydrogen enhanced localized plasticity and decohesion [4].

Hydrogen enters dislocations generated during straining and diffuses further into the material during the SSRT testing as shown in literature [4,11]. The tested charged samples which are fully hydrogen saturated can be a cause for the reduction of strain after onset of yielding by promoting "intergranular" cracking along the prior austenite grain boundaries [4]. The intergranular cracking along the prior austenite grain boundaries greatly reduces the strain hardening of hydrogen charged samples. This is demonstrated in this study where the first crack tends to increase to a critical size and is formed in the region of the prior austenite grain boundaries. At lower temperatures, hardness, yield and tensile strengths are quite high and consequently it may initiate a small crack that leads to a high stress concentration factor. The bonds between the prior austenite grain boundaries are weaker than the boundaries between martensitic laths. The width of martensitic lath, dislocation density and carbide precipitates can affect mechanical properties of the material [43]. The coarsening of carbides at higher tempering temperature and carbon content reduce the tensile strength and the rate of strain hardening [44]. This may be the cause for the very low work hardening rate for hydrogen uncharged samples, tempered at 460 °C and higher, and the samples tempered at 520 °C and higher (Fig. 5).

The critical stress around 1200 MPa for crack initiation and propagation is less than the yield stress for all the charged and tempered states at temperatures below 460 °C. Interestingly, when the tensile strength

for the non-charged and charged samples reaches the same level, around 1200 MPa at 460 °C, the susceptibility index for hydrogen embrittlement drops. At higher temperatures, the yield strength of the charged samples decreases, and elongation increases with increasing temperature. The fracture surface tends to have more ductile behaviour with spherical dimples for the samples tempered at highest temperature (Fig. 8(f)).

The elongation for non-charged samples becomes substantially longer. In addition to tempering, the mechanisms leading to hydrogen embrittlement need to be considered to understand the irregularity of yield strength and elongation. Solubility and diffusion rate and ductility near crack at different temperatures should be addressed to understand the phenomenon.

The HE susceptibility of AISI 4130 steel increased with increasing hardness (i.e. decreasing tempering temperature) as shown in Figs. 6 and 7. Hydrogen traps are characterized by the trapping energy. Dislocations are typically low energy traps, which will allow hydrogen to diffuse at room temperature. Coherent precipitates may also result in low energy traps and increased solubility due to the distortion of the surrounding atomic lattice. The amount and nature of precipitates can thus influence the hydrogen solubility and diffusion, and hence may affect HE susceptibility. The mobile hydrogen is mainly trapped by dislocations and governed the HE susceptibility [11]. In general, the results from this study agree with previous reports [13,41] that showed susceptibility of AISI 4130 to HE when the hardness of the material is high (at lower tempering temperature). In contrast, when tempering temperature increases, the resistance to HE increases. The mobile and diffusible hydrogen may not influence the elastic behaviour of hydrogen charged samples as the slope of stress-strain curves were not changed due to tempering temperature [45].

4.2. Effect of tempering temperature on the fracture behaviour and microstructure

It is generally accepted that increased hardness in steel increases the hydrogen cracking susceptibility because increased hardness increases the local stresses at irregularities in the material and thus the driving force for hydrogen diffusion to these areas. However, dislocation density is considerably high when the steel is as quenched state but reduced after the steel is tempered. Thus, the concentration of trapped hydrogen is lowered with increasing tempering temperature [4,39]. An increase in trapped hydrogen may therefore be the reason for a higher amount of developed intergranular cracks in the tempered martensitic steel at lower temperature as described in Section 3.4. In contrast, a ductile fracture behaviour with dimples may be observed for the hydrogen charged samples with higher tempering temperature [4,39]. These observations support the conclusion made above, i.e. AISI 4130 material is subjected to HE susceptibility due to hydrogen charging, when the hardness is increasing.

As shown in Figs.9 to 11, the as quenched and tempered martensitic steel microstructure consists of prior austenite grain boundaries, martensitic lath boundaries and carbide-matrix interfaces. The diffused hydrogen is trapped near the crack tips and helps to propagate the cracks. The high amount of hydrogen near the crack tips can be considered as one of the factors responsible for the propagation of the cracks. Even though hydrogen causes the embrittlement, strain rate, local stress concentrations and microstructure have substantial influences on the embrittlement.

5. Conclusions

Susceptibility to Hydrogen embrittlement (HE) of the tempered and hydrogen charged high strength carbon steel, AISI 4130, was investigated by slow strain rate tensile test (SSRT). Microstructural characterization and fracture surface examination were done in order to study the effects of hydrogen in relation to embrittlement. The following conclusions are made from the study.

- When hardness is larger than 465 HV (corresponding to tempering temperature less than 430 °C):
  - The HE susceptibility index of reduction of cross-sectional area and fracture strain (i.e. strain to failure) are about 100% and 80%, respectively.
  - The as quenched samples experienced the highest hydrogen embrittlement susceptibility and are subjected to intergranular cracking due to hydrogen charging.
  - The percentage reduction of cross-sectional area is negligible.
  - The fracture surface examination showed transition of ductile microvoid coalescence to brittle intergranular cracking.
- The limiting tensile strength (ultimate tensile strength) and fracture strain (ultimate fracture strain) can be conservatively considered as 1200 MPa and 0.02, respectively for hydrogen pre-charged high strength carbon steel, AISI 4130.
- The fracture behaviour is ductile and hydrogen embrittlement susceptibility decreases when tempering temperature is higher than 490 °C.
- Generally, the hydrogen charged high strength carbon steel, AISI 4130 is 100% susceptible to HE when the hardness is larger than 465 HV.

In general, more than one test should be performed to have statistically valid relevant data. Therefore, detailed investigation of HE susceptibility of AISI 4130 with hardness value 450–500 HV is recommended using many samples in the same test condition for further validation/confirmation of the obtained limiting values.

The discussion has been done in this study based on trapped hydrogen and increased hydrogen concentrations for specimens tempered at a lower temperature to support the above conclusions made, which were based on SSRT test results. However, hydrogen saturation has not been checked for every material condition by determining the hydrogen concentration at different charging times. Therefore, the authors have recommended more quantitative assessment of trapped hydrogen by thermal desorption spectroscopy measurements or through hot extraction of AISI 4130 steel with hardness value of 450–500 HV.

CRediT authorship contribution statement

Nirosha D. Adasooriya: Conceptualization, Methodology, Investigation, Formal analysis, Visualization, Writing - original draft. **Wakshum Mekonnen Tucho:** Methodology, Investigation, Formal analysis, Writing - review & editing. **Erlend Holm:** Methodology, Investigation, Writing - review & editing. **Terje Årthun:** Methodology, Investigation, Writing - review & editing. **Vidar Hansen:** Conceptualization, Methodology, Formal analysis, Writing - review & editing, Supervision, Resources. **Karl Gunnar Solheim:** Conceptualization, Methodology, Formal analysis, Writing - review & editing, Supervision, Resources. **Tor Hemmingsen:** Conceptualization, Methodology, Formal analysis, Writing - review & editing, Supervision, Resources.

Declaration of competing interest

The authors declare that they have no known competing financial interests or personal relationships that could have appeared to influence the work reported in this paper.

Acknowledgement

The authors would like to thank Johan Andreas Thorkaas, Adugna Deressa Akessa, Mona Minde, Tor Gulliksen, Jan Magne Nygård and John Grønli for their support in the labs. Erlend Sølvberg from Kverneland Group is highly appreciated for conducting the heat treatments.

Appendix A. Supplementary data

Supplementary data to this article can be found online at https://doi.org/10.1016/j.msea.2020.140495.

References

[1] K. Gjerding-Smith, R. Johnsen, H.I. Lange, B.H. Leinum, G. Gundersen, B. Isaksen, G. Nærum, Wire fractures in locked coil cables, Bridge Structures Assessment, Design and Construction 2 (2007) 63–77.
[2] J.M. Kulicki, Z. Prucz, D.F. Sorgenfrei, W.T. Young, Guidelines for Evaluating Corrosion Effects in Existing Steel Bridges, Transportation Research Bboard National Research Council, Washington, D.C., 1990.
[3] Y. Cung, L.K. Fulton, Environmental hydrogen embrittlement of G41400 and G43400 steel bolting in atmospheric versus immersion services, J. Fail. Anal. Prev. 17 (2017) 330–339.
[4] B.S. Kumar, V. Kain, M. Singh, B. Vishwanadh, Influence of hydrogen on mechanical properties and fracture of tempered 13 wt% Cr martensitic stainless steel, Mater. Sci. Eng. A700 (2017) 140–151.
[5] I.M.E. Aghoury, K. Galal, Corrosion-fatigue strain-life model for steel bridge girders under various weathering conditions, J. Struct. Eng. 140 (2014). Article no: 04014026.
[6] I.E. Aghoury, Numerical Tool for Fatigue Life Prediction of Corroded Steel Riveted Connections Using Various Damage Models, PhD Thesis, Concordia University, Canada, Montreal, 2012.
[7] P. Roberge, Handbook of Corrosion Engineering, McGraw Hill, 2000.
[8] R.W. Revie, H.H. Uhlig, Corrosion and Corrosion Control, an Introduction to Corrosion Science and Engineering, Wiley and Sons, 2008.
[9] G.P. Tiwari, A. Bose, J.K. Chakravartty, S.L. Wadekar, M.K. Totlani, R.N. Arya, R. K. Fotedar, A study of internal hydrogen embrittlement of steels, Mater. Sci. Eng. 286 (2000) 269–281.
[10] C.L. Lai, L.W. Tsay, C. Chen, Effect of microstructure on hydrogen embrittlement of various stainless steels, Mater. Sci. Eng. 584 (2013) 14–20.
[11] T. Depover, K. Verbeke, Hydrogen trapping and hydrogen induced mechanical degradation in lab cast Fe-C-Cr alloys, Mater. Sci. Eng. 669 (2016) 134–149.
[12] Y. Zheng, F. Wang, C. Li, Y. Lin, R. Cao, Effect of martensite structure and carbide precipitates on mechanical properties of Cr-Mo alloy steel with different cooling rate, High Temp. Mater. Process. 28 (2019) 113–124.
[13] N. Nanninga, J. Grochowsi, L. Heldt, K. Rundman, Role of microstructure, composition and hardness in resisting hydrogen embrittlement of fastener grade steels, Corrosion Sci. 52 (2010) 1237–1246.
[14] V.H.B. Hernandez, S.S. Nayak, Y. Zhou, Tempering of martensite in dual-phase and its effect on softening behavior, Metall. Mater. Trans. 42 (2011). Article number: 3115.
[15] L. Marchetti, E. Herma, P. Laghoutaris, J. Chêne, Hydrogen embrittlement susceptibility of tempered 9%Cr–1%Mo steel, Int. J. Hydrogen Energy 36 (2011) 15880–15887.
[16] T. Das, S.K. Rajagopalan, S.V. Brahimi, X. Wang, S. Yue, A study on the susceptibility of high strength tempered martensite steels to hydrogen embrittlement (HE) based on incremental step load (ISL) testing methodology, Mater. Sci. Eng. 716 (2018) 189–207.
[17] M.B. Djukic, G.M. Bakic, V.S. Zeravcic, B. Rajicic, A. Sedmak, R. Mitrovic, Z. Miskovic, Towards a unified and practical industrial model for prediction of hydrogen embrittlement and damage in steels, Procedia Structural Integrity 2 (2016) 604–611.
[18] M.B. Djukic, V.S. Zeravcic, G.M. Bakic, A. Sedmak, B. Rajicic, Hydrogen damage of steels: a case study and hydrogen embrittlement model, Eng. Fail. Anal. 58 (2015) 485–498.
[19] D.P. Escobar, C. M, L. Duprez, K. Verbeken, M. Verhaege, Internal and surface damage of multiphase steels and pure iron after electrochemical hydrogen charging, Corrosion Sci. 53 (2011) 3166–3176.
[20] G. Biggiero, A. Borruto, I. Taraschi, Effects of hydrogen charging methods on ductility and fracture characteristics of AISI 9840 steel, Int. J. Hydrogen Energy 20 (1995) 465–470.
[21] Q. Liu, A.D. Atrens, Z. Shi, K. Verbeken, A. Atrens, Determination of the hydrogen fugacity during electrolytic charging of steel, Corrosion Sci. 87 (2014) 239–258.
[22] T. Michler, J. Naumann, Microstructural aspects upon hydrogen environment embrittlement of various BCC steels, Int. J. Hydrogen Energy 35 (2010) 821–832.
[23] NORSOK M-001, Materials Selection, NTS, 2003.
[24] J.L. Battle, T.V. Miller, M.E. True, Resistance of commercially available high strength tubular goods to sulfide stress cracking, Am. Soc. Mech. Eng. 14 (1975) 11–22.
[25] M. Gao, P. Wei, A, Hydrogen partitioning model for hydrogen assisted crack growth, Metallurgical Transactions A 16 (1985) 2039–2050.
[26] H. Lee, S.L. Chan, Hydrogen embrittlement of AISI 4130 steel with an alternate ferrite/pearlite banded structure, Mater. Sci. Eng. 142 (1991) 193–201.
[27] L. Vergani, C. Colombo, G. Gobbi, F.M. Bolzoni, G. Fumagalli, Hydrogen effect on fatigue behavior of a quenched & tempered steel, in: 17th International Colloquium on Mechanical Fatigue of Metals, ICMFM, 2014. Verbania, Italy, Procedia Engineering 74 (2014) 468-471.
[28] G. Gobbi, C. Colombo, L. Vergani, A cohesive zone model to simulate the hydrogen embrittlement effect on a high-strength steel, Fracture and structural Integrity 10 (2016) 260–270.
[29] I.C.C. Gobbi, L. Vergani, Sensitivity analysis of a 2D cohesive model for hydrogen embrittlement of AISI 4130, Eng. Fract. Mech. 167 (2016) 101–111.
[30] H. Chumalo, M. Student, B. Datsko, Y. Kharchenko, Some ways to ensure reliable operation of oil and gas equipment in hydrogen sulfide environment, J. Corrosion Sci. Eng. 21 (2018).
[31] NS-EN ISO 6507-1, Metallic Materials – Vickers Hardness Test - Part 1: Test Method, Norsk Standard, Standard Online AS, 2018.
[32] ASTM G 129-00, Standard Practice for Slow Strain Rate Testing to Evaluate the Susceptibility of Metallic Materials to Environmentally Assisted Cracking, ASTM Internationals, 2013.
[33] A. Jemal, M. Birihane, Hydrogen Embrittlement in High Strength Carbon Steel AISI 4130, Mater Thesis, University of Stavanger, 2017.
[34] Y. Zhang, W. Hui, X. Zhao, C. Wang, H. Dong, Effects of hot Stamping and tempering on hydrogen embrittlement of a Low- carbon Boron-Alloyed steel, Materials 11 (2018). Article number: 2507.
[35] S. Shen, X. Song, Q. li, X. LI, R. Zhu, G. Yang, A study on stress corrosion cracking and hydrogen embrittlement of Jethete M152 martensitic stainless steel, Mater. Sci. Eng. 740–741 (2019) 243–251.
[36] NS-EN ISO 6892-1, Metallic Materials - Tensile Testing - Part 1: Method of Test at Room Temperature, Norsk Standard, Standard Online AS, 2009.
[37] Preparation of ferrous metals Struers application notes. https://www.struers.com/en/Material.
[38] Bruce D. Crajg, George Krauss, The structure of tempered martensite and its susceptibility to hydrogen stress cracking, Metallurgical Trans. A 11A (1980) 1799–1808.
[39] S. Lee, A. Joseph, Ronevich, G. Krauss, D.K. Matlock, Hydrogen embrittlement of hardened low carbon sheet steel, ISIJ Int. 50 (2010) 294–301.
[40] W. Lee, T. Su, Mechanical properties and microstructural features of AISI 4340 high-strength alloy steel under quenched and tempered conditions, J. Mater. Process. Technol. 87 (1999) 198–206.
[41] L.D. Barlow, M.D. Toit, Effect of austenitizing heat treatment on the microstructure and hardness of martensitic stainless steel AISI 420, J. Mater. Eng. Perform. 21 (2012) 1327–1336.
[42] A.R. Troiano, The role of hydrogen and other interstitials in the mechanical behavior of metals, Metallography, Microstructure, and Analysis 5 (2016) 557–569.
[43] D. Zhao, S. Zhang, H. Zhang, S. Li, H. Xiao, Y. Wang, X. Wang, Effects of tempering temperature on the microstructure and mechanical properties of T92 heat-resistant steel, Metals 9 (2019) 194, https://doi.org/10.3390/met9020194.
[44] G. Krauss, D. Matlock, Effects of strain hardening and fine structure on strength and toughness of tempered martensite in carbon steels, Journal de Physique IV Colloque (1995) 51–60, 05 (C8).
[45] M. Wang, E. Akiyama, K. Tsuzaki, Effect of hydrogen on the fracture behavior of high strength steel during slow strain rate test, Corrosion Sci. 49 (2007) 4081–4097.